International Forum on Aeroelasticity and Structural Dynamics
IFASD 2024
17-21 June 2024, The Hague, The Netherlands

A CFD/CTD/CSD BASED AERO-THERMO-ELASTIC FRAMEWORK FOR FULL-VEHICLE SCALE ANALYSIS

Liang Ma[1], Zhiqiang Wan[1], Xiaozhe Wang[*,2], Keyu Li[1], Chang Li[1], and Longfei He[3]

[1] School of Aeronautic Science and Engineering, Beihang University, 37 Xueyuan Road, Haidian District, Beijing, P.R. China, 100191.
[2] Institute of Unmanned System, Beihang University, 37 Xueyuan Road, Haidian District, Beijing, P.R. China, 100191.
[3] China Academy of Launch Vehicle Technology, Beijing, P.R. China, 100191.

Keywords: Hypersonic, aero-thermo-elasticity, partitioned loose coupling strategy, CFD method, FEM method

Abstract: Due to the significant multidisciplinary coupling mechanism inherent in hypersonic flight mission, unnecessary and wasteful trade-off in vehicle performance will be cost if complex load distribution and aerodynamic heating effect are neglected at the early stage of design. This paper establishes an CFD/CTD/CSD based aero-thermo-elastic framework for analysis of the full-vehicle scale. The loose coupling strategy is chosen in this framework to reveal the specific efforts of each disciplinary, and the RBF-TFI method is introduced for mesh deformation. This study is carried on the rudders assembled on a hypersonic missile, with the high-fidelity aerodynamic data of the full-vehicle model extracted by CFD and only the component deformation of the rudders extracted by FEM. This paper demonstrates the aero-thermo-elastic effects of those factors concealed by engineering algorithms, with the influence mechanism revealed from the results discussed.

1 INTRODUCTION

Hypersonic vehicles refer to those designed to fly at speeds of 5 Ma and above, which will bring about great changes in cosmic exploration, business travel and homeland security[1,2]. With great scientific research value in this area, hypersonic research has long been of great interest to various countries, and in recent years, it has developed rapidly driven by the development of relevant technologies.

Different from the common vehicles with subsonic or supersonic speeds as the goal of design conditions, design of hypersonic vehicles is more complex due to the special characteristics of the operating environment and mission profile[1]. Many challenges are posed to the relevant technical means. Hypersonic flow (Ma>=5) is usually characterized by strong shock wave and significant aerodynamic heat[3]. On the one hand, the presence of extreme aerodynamic pressure and heat in hypersonic flows significantly alters the flow characteristics. The large difference in heat transfer between laminar and turbulent boundary layers, shock wave/boundary layer interaction, etc. impose aerodynamic load on the structure and significantly enhance the heat transfer effects[4]. On the other hand, in addition to the effect of the flow field itself, the structural surface of the

vehicle also has a significant effect on the surrounding high-temperature flow. Structural steps and gaps may trigger the boundary layer, leading to downstream transition or turbulent flows with significantly higher heat fluxes[5], and the high pressure and temperature in near-wall hypersonic flow may lead to ionization reactions of gases, resulting in aerodynamic heating uncertainties[6]. These phenomena, however, are difficult to predict accurately by conventional engineering algorithms.

The effects of hypersonic flow on structures are dominated by aerodynamic heating and pressure load[7]. The high Mach number and long flight range make the coupling between structural heat transfer and structural stress/strain field extremely strong. Sustained hypersonic flight induces severe aerodynamic heating, which leads to an increase in structural temperature and degradation of material properties[8,9]. Meanwhile, thermal stress introduced by temperature gradients and geometrical constraints has a significant impact on structural integrity, generating thermal stress in the structure, creating thermal deformation and weakening structural stiffness[5,10], which may lead to dangerous structural response behaviors, such as buckling and fluttering[11,12]. Therefore, structural response analysis under thermal and pressure load, also known as aero-thermo-elastic analysis, is essential for design of hypersonic vehicles.

Accurate sources of aerodynamic and aerothermal data are usually results from the computational fluid dynamics (CFD) numerical simulations or wind-tunnel tests. Due to the difficulty of wind-tunnel tests, the fluid-thermal-structure interaction (FTSI) numerical simulation method based on CFD and the finite element method (FEM), which contains computational structural dynamics (CSD) and computational thermodynamics (CTD), is an important tool for aero-thermo-elastic analysis. Researchers used to make a constant temperature distribution assumption for structural thermodynamic analysis. There have been also engineering algorithms with more restrictive assumptions used to evaluate the structural surface temperature field[13]. Nowadays researchers in various countries are paying more attention to the impact of accurate FTSI modeling on the analysis of aero-thermo-elasticity problems and the optimal design of hypersonic vehicles. There is an increasing of studies using accurate CFD as a means of analyzing aerodynamic heating effects[14–17].

In summary, the CFD/CTD/CSD based FTSI method for multi-field coupling analysis of hypersonic vehicles is of great research significance. As far as the authors of this paper know, the influence of the complex real situations of hypersonic vehicles, especially the assembly state, on the aero-thermo-elastic phenomena has not been widely discussed yet. Therefore, the object in this paper is the rudders assembled on a missile body. An aero-thermo-elastic framework for static analysis of the assembled rudder components is established. The aim of this paper is to explore the specific guidance that such technical tools can provide in hypersonic vehicle design. The subsequent parts of this paper are organized as follows: Section 2, which introduces the basic theory of aero-thermo-elasticity; Section 3, which introduces the aero-thermo-elastic analysis framework constructed in this paper and validates it using a simple rudder example; Section 4, using the framework in Section 3, in which a static aero-thermo-elastic analysis of the rudders under the fully-assembled state with time-dependent thermal accumulation is carried out, and the simulation results obtained are discussed; and Section 5, which summarizes the whole paper.

2 BASIC THEORIES FOR AERO-THERMO-ELASTIC ANALYSIS FRAMEWORK

The hypersonic aero-thermo-elastic problem is a multidisciplinary coupled problem that integrates the disciplines of aerodynamic heating, aerodynamic loading, and structural thermodynamics. It is usually divided into two parts[18]: 1) aerothermal problem; and 2) aeroelastic problem. Aerothermal analysis consists of aerodynamic heating calculation and heat conduction calculation, which show the heat flux on structural surfaces and the temperature distribution of the whole structure, where the aerodynamic heat flux is a function of the temperature of structural surfaces and the aerodynamic load distribution. Aeroelastic analysis shows the deformation of the structure, under both the aerodynamic loading and aerodynamic heating, and this geometrical change induces the change in the aerodynamic load distribution. It can be seen that there exist complex coupling relationships among the various subdisciplines of aerodynamics, aerodynamic heat, heat transfer and structural dynamics in the hypersonic aero-thermo-elastic problem, and the strength of these coupling effects varies, as shown in Fig. 1.

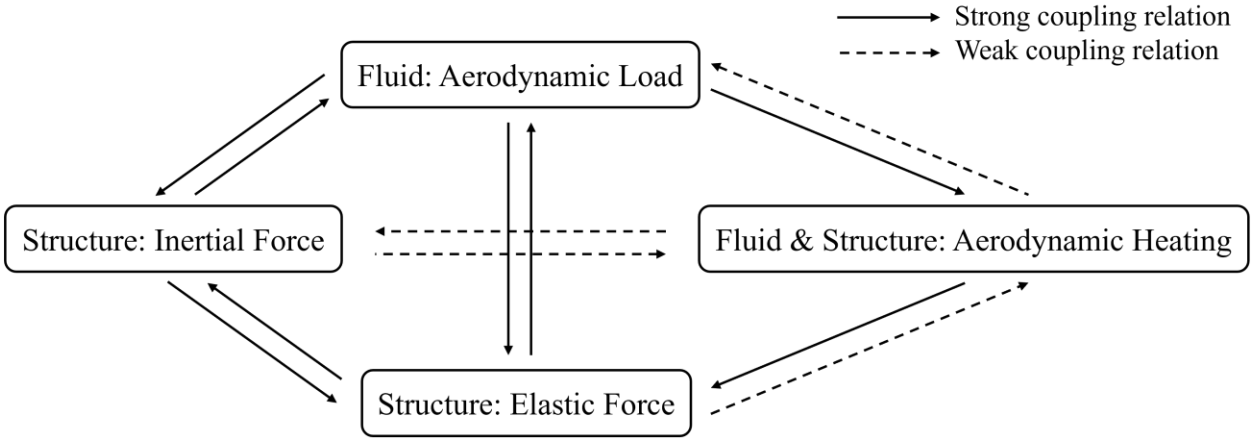

Fig. 1 Strong and weak coupling relations in aero-thermo-elastic problem

In subsonic and many problems of low supersonic speed, the coupling effect between the subdisciplines above is very weak, and the method of independent subdiscipline analysis is commonly used to study them. However, for hypersonic problems with significant multidisciplinary coupling effects, the consideration of the interactions between the subdisciplines has a great impact on the correctness of the conclusions, so a multidisciplinary coupling analysis is very necessary.

The complex FTSI problem under hypersonic speed can be divided into strong and weak coupling from physical meaning level. The weak coupling relations in Fig. 1 are usually ignored, and the aero-thermo-elastic studies only focus on the strong ones. The following three assumptions are often used when performing this type of analysis:

1) The heat generated by structural deformation is considered to be small and negligible;

2) The time scale of the aerothermal problem is much larger than the response period of the aeroelastic problem;

3) The degree of aeroelastic-thermal coupling is low and the elastic deformation is not sufficient to change the structural temperature distribution.

As shown in Fig. 2, there are two types of integrated and partitioned solutions to deal with the strong effects, especially for the aerodynamic heating. The partitioned solution can be further divided into one-way coupling and two-way coupling strategies. Both of the partitioned strategies can be divided into loose coupling and tight coupling from the level of the computational method of the aeroelasticity sub-problem.

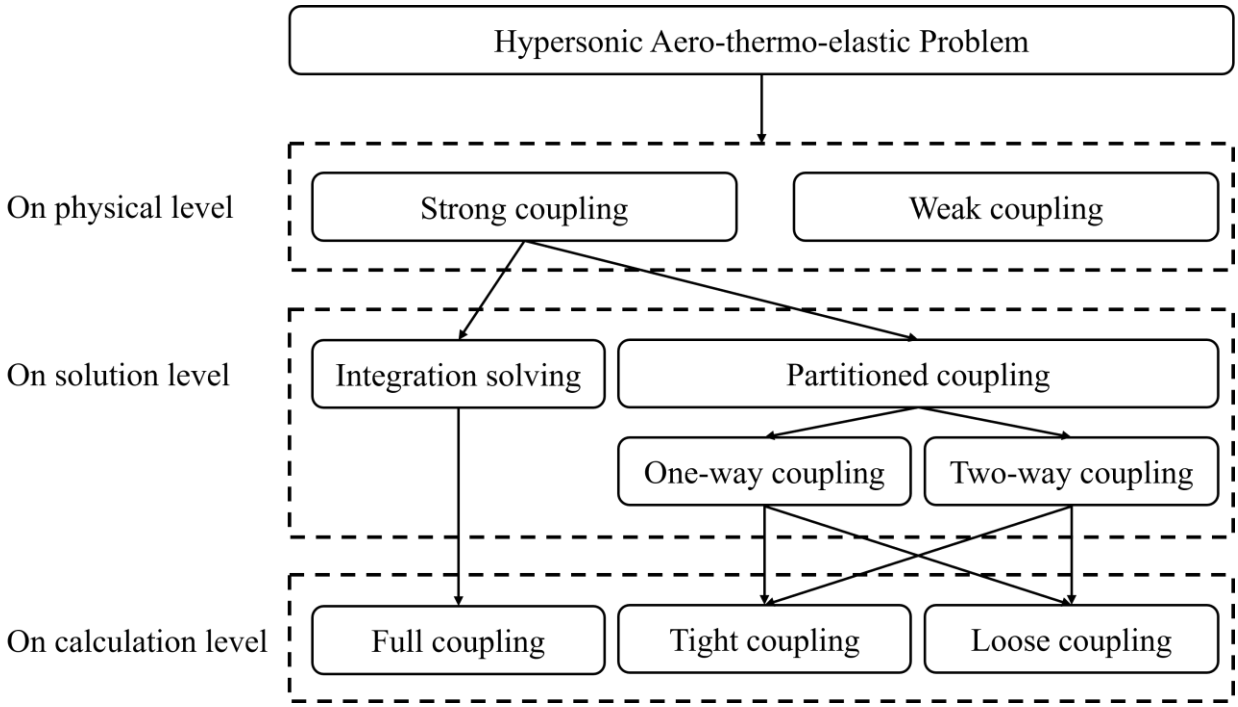

Fig. 2 Analytical hierarchy of aero-thermo-elastic problem

2.1 Integration solving and partitioned coupling

For aero-thermo-elastic problems under lower flight speed and those where the aerodynamic heating effect is considered to be less important, studies usually analyze it in a fully-coupled partial differential equation with the integrated strategy, in which aerodynamic load and heat flux on structural surfaces are coupled into the unified governing equation, treating the fluid effects at its interface with the structure as boundary conditions for the governing equation. And the effects of heat transfer are captured by the temperature-influenced matrix parameters. This governing equation is usually established by Hamilton's principle, and is discretized by Galerkin method, assumed mode method, Generalized Differential Quadrature(GDQ) method and other methods, and solved in the time or frequency domain[19–22]. This strategy couples all the related sub-disciplines through one governing equation and solves all the disciplines at one time. The physical meaning of the results is clear and precise, and therefore of theoretical interest.

However, for complex problems, such as complex structural models, complex flow fields, etc., those simplified and analytical engineering algorithms that have been employed to establish the fully-coupled governing equations are no longer applicable. Researchers have to develop a new

approach of transferring data between subdisciplines and analyzing each subdiscipline separately. This strategy of obtaining multidisciplinary coupling results through iterative convergence is known as the partitioned coupling strategy.

Due to the separate modeling and analysis of each subdiscipline, the partitioned coupling strategy can take different time steps for the aeroelasticity problem and heat conduction problem, which is closer to the real multi-field coupling phenomenon[11,20,23,24], through which, researchers can carry out the analysis of the time accumulation, fully consider the anisotropy of the structural materials as well as thermal stress and thermal deformation, and take the high-temperature real gas effect into account, etc.

2.2 One-way coupling and two-way coupling

The partitioned coupling strategy can be subdivided into one-way coupling and two-way coupling according to the consideration of the retained strong influence of physical couplings.

The one-way coupling firstly predicts the aerodynamic heat and load distribution on the vehicle surface, then calculates the structural dynamics of the vehicle under the thermal environment. The aeroelastic solution it carries out, with the effect of structural deformation on the aerodynamic force and heat ignored. One-way coupling decouples the aerodynamic heat, heat transfer and aeroelasticity solving from each other, making it possible to analyze each subdiscipline independently. But the results of the analysis of some problems may be greatly deviated from the actual situation.

The two-way coupling needs to consider the feedback effect of structural deformation on aerodynamic heat and force on the basis of one-way coupling. Therefore, it is required to consider aerodynamic heating, heat conduction and aeroelasticity at the same time, which is relatively complex, but it can fit the actual situation to a greater extent, and reduce the analysis error.

2.3 Tight coupling and loose coupling

For the specific solution of the aeroelastic sub-problem, there are two different computational methods, namely, loose coupling and tight coupling.

The tight-coupling method establishes a unified aeroelastic equation under the partitioned coupling strategy for aerothermal sub-problem. Like the full-coupling, it also requires a more simplified method for aerodynamic solution in order to express the governing equation easily. So tight-coupling has the advantages similar to the full-coupling, i.e., the physical meaning is clear, which makes it easy for the researcher to grasp the key of the problem, and is faster to calculate.

The loose coupling method is to solve the aeroelastic subproblem by iterative calculations among sub-disciplines, maximizing the advantage of high accuracy of the partitioned coupling. However, those high-precision methods, such as CFD, makes the computation period elongated and the result shows no explicit physical meaning.

Since the loose coupling method supports high-precision CFD solution of aerodynamic and aerothermal problems, which is the only available method for the complex flow field of the assembly studied in this paper, the aero-thermo-elastic analysis framework established in this paper adopts the partitioned loose coupling method to model each sub-discipline separately.

3 THE AERO-THERMO-ELASTIC FRAMEWORK AND ITS VERIFICATION

This paper establishes an analysis framework based on the partitioned two-way loose coupling method, in which the CFD method is introduced to solve aerodynamic load and aerodynamic heating, with the CTD method for linear structural heat transfer analysis and CSD for linear structural static analysis. All of them are well-developed sub-disciplinary analysis methods, so there is no detailed introduction in this section, only a description of specific settings.

3.1 The aero-thermo-elastic framework established

The analysis framework in this paper, as shown in Fig. 3, is mainly composed of nested two-layer iterative loops and three sub-disciplinary analysis modules. The time-driven thermal environment analysis is the external cycle, and the aeroelastic convergence is the internal cycle. Three sub-disciplinary analysis modules are composed of CFD-based aerothermal dynamics analysis, CTD-based thermal environment analysis and CSD-based structural mechanic analysis respectively. The analysis steps are as follows:

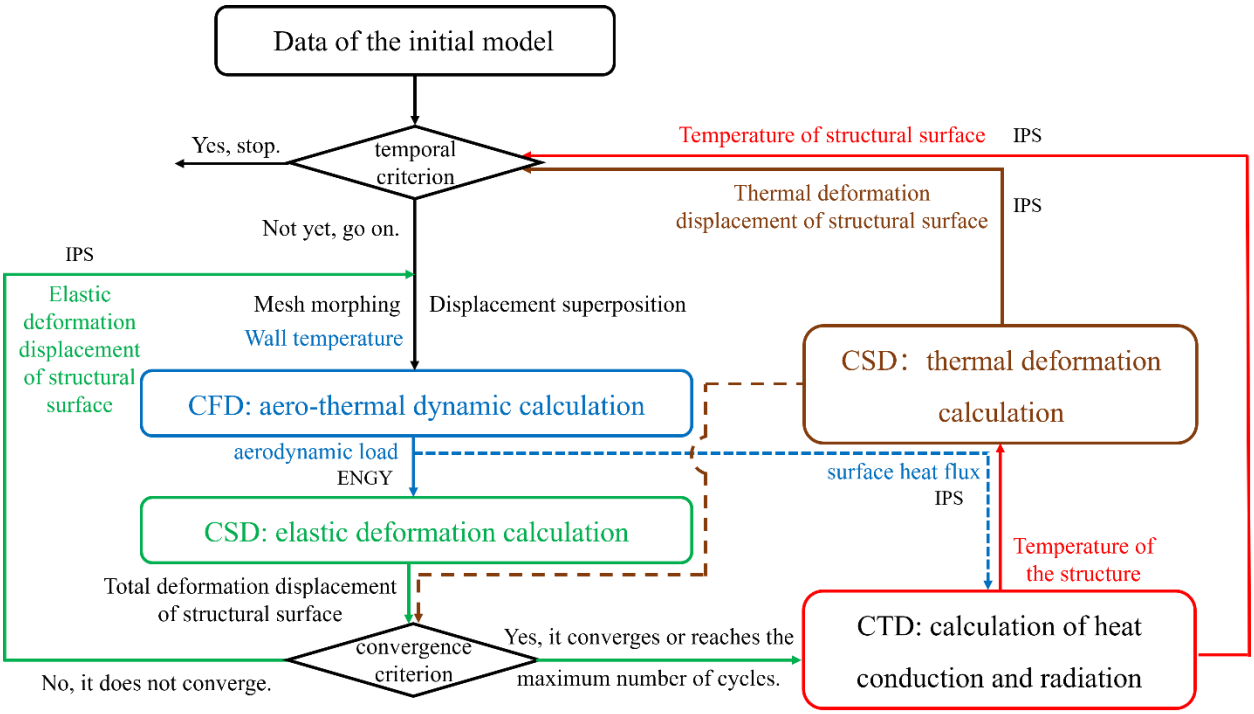

Fig. 3 Flow chart of the aero-thermo-elastic analysis framework

1) The initial model, including the structural position and temperature distribution, is given.

2) Carry out the aeroelastic inner cycle until the maximum number of executions of the small cycle or the displacement convergence condition is reached. First, the rigid CFD operation is performed to obtain the distribution of the aerodynamic load on the structural surface under the given total displacement and temperature condition. Then, the structural mechanic analysis is performed to obtain the elastic deformation of the structure.

3) Carry out the thermal environment outside cycle, and the thermal accumulation effect is promoted according to the given time step. First, the structural heat transfer and heat radiation analysis is carried out to obtain a new structural temperature distribution under the condition

of the surface temperature distribution and surface heat flux given by CFD. Through the equivalent thermal load, carry out structural mechanic analysis again for the structural thermal deformation.

4) Update the model. Superimpose the thermal deformation displacement with the elastic deformation displacement to shape a new structural position. The temperature results of heat transfer analysis are used as the temperature condition for new cycles.

3.1.1 CFD module

The flow field analysis module is introduced in this framework to solve the rigid aerodynamic force and heat flux on the rudder in the case of a full-missile assembly. The fluid mesh is modeled by the overlapping mesh method, with each component is a hexahedral structured mesh. The mesh file used for CFD calculations is a combination of the right half-mode background mesh containing the wall boundaries of the missile body and the component meshes for the two rudders located on its right side. The steady-state hypersonic flow is calculated implicitly with double precision using a compressible ideal gas model and a one-equation S-A turbulence model. The initial aerodynamic shape and overlapping mesh used in CFD are shown in Fig. 4. All boundary conditions involved are shown in Tab. 1.

Tab. 1 Boundary conditions

Mesh Group	Boundary description	Boundary condition
Background mesh for the body	Inflow surfaces	Supersonic Inflow
	Outflow surfaces	Centroidal Extrapolation
	Symmetry plane of the body	Symmetry
	Wall surfaces of the body	Viscous (No-Slip) Wall Isothermal Wall at 300K
Component mesh for one of the rudders	Outer surfaces of the component mesh	Overset
	Wall surfaces of the rudder	Viscous (No-Slip) Wall Isothermal Wall based on CTD result

3.1.2 CTD and CSD module

For the structural elastic deformation and thermal deformation analysis modules, as well as the heat transfer module, the finite element model of the rudder structure with root fixed support is made and shown in Fig. 5, with the material parameter settings given in Tab. 2.

The control equation for heat transfer is

$$q_n = -k_n \frac{\partial T}{\partial n} \tag{1}$$

in which, q_n is the heat flux density, $\frac{\partial T}{\partial n}$ is the normal temperature gradient, with k_n is the thermal conductivity in that direction. In order to determine the solution of this equation, the

Neumann boundary condition (the heat flux density at the boundary of the object) and the initial condition (the temperature distribution of the whole object) are given.

The thermal radiation from the structural surfaces is calculated by the following equation:

$$Q_{rad} = \sigma\varepsilon(T_w{}^4 - T_\infty{}^4) \tag{2}$$

where T_w is the wall temperature, T_∞ is the temperature at infinity, $\varepsilon = 5.669E^{-8}W/m^2/T^4$ is the Stanford constant, and σ is the non-blackbody surface emissivity, which is constant 0.85 to simplify the analysis in this paper. The heat flux output of CFD, Q_{aero}, is the aerodynamic heating, so for the CTD module, the final heat flow into the structure is $Q = Q_{aero} - Q_{rad}$. In this paper, FEM is used to discretize the linear solution of (1).

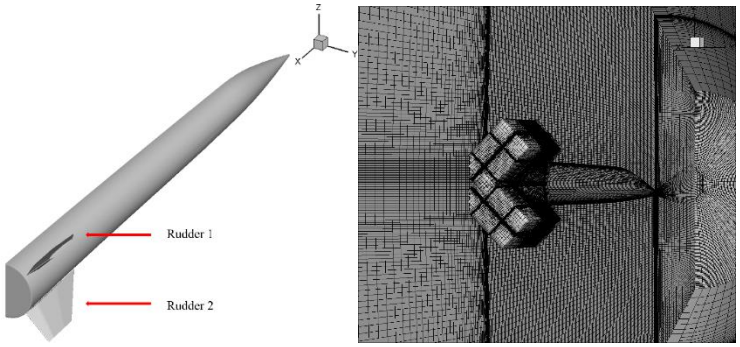

Fig. 4 Aerodynamic model for CFD (left: aerodynamic model; right: overlapping mesh)

Tab. 2 Material parameter settings

TIMETAL 834	Density	$4.55*10^{-6}\text{kg/mm}^3$
	Young's modulus	$\approx[-75656/\text{K}*(T-293\text{K})+1.09*10^8]\text{kg/mm/s}^2$
	Poisson's ratio	0.31
Rene 41 protection	Density	$2.56*10^{-7}\text{kg/mm}^3$
	Young's modulus	$1.09*10^8\text{kg/mm/s}^2$
	Poisson's ratio	0.31
Min-K insulation	Density	$8.24*10^{-6}\text{kg/mm}^3$
	Young's modulus	$1.09*10^8\text{kg/mm/s}^2$
	Poisson's ratio	0.31

Based on the static equilibrium equation of the 3D linear elastic structure, the finite element integral equation for the FEM static analysis of the structure can be obtained according to the principle of virtual work as

$$\mathbf{KU = F} \tag{3}$$

where $\mathbf{K}$ is the assembled stiffness array, $\mathbf{U}$ is the assembled displacement vector, and $\mathbf{F}$ is the assembled load vector obtained by combining various boundary conditions. The assembled stiffness array $\mathbf{K}$ is mainly obtained by assembling the element stiffness array of each cell

$$\mathbf{K} = \sum_{e} \int_{\Omega_e} \mathbf{B}^{\mathrm{T}} \mathbf{D} \mathbf{B} \tag{4}$$

where $\mathbf{B}$ is the linear strain matrix and $\mathbf{D}$ is the stress-strain relationship matrix in the linear constitutive equation in this paper. After solving (3) to obtain the assembled displacement result, the strain and stress distribution of the structure can be obtained based on the geometric and intrinsic equations in turn.

For the assembled finite element equation, the thermal strain due to the temperature gradient corresponds to the addition of a thermal stress loading term to the right-hand end of the original static equilibrium equation of the structure, which is called the equivalent thermal load.

$$\mathbf{KU} = \mathbf{F} + \sum_{e} \int_{\Omega_e} \mathbf{B}^{\mathrm{T}} \mathbf{D} \boldsymbol{\varepsilon}_T = \mathbf{F} + \mathbf{F}_T \tag{5}$$

where $\boldsymbol{\varepsilon}_T$ is the assembled thermal strain matrix and $\mathbf{F}_T$ is the thermal load.

In this paper, thermal load and aerodynamic load are considered separately, using the linear static analysis method to solve their corresponding structural displacement, namely elastic deformation displacement and thermal deformation displacement respectively.

3.2 Other supporting technologies and methods

The analysis of aero-thermo-elastic problems using a loose coupling approach requires data interpolation techniques to transfer the results from each sub-discipline to other and mesh morphing techniques to continuously update the geometry of the CFD mesh, as shown in Fig. 6. There are many well-developed methods for both data interpolation and mesh morphing, this section mainly provides a brief description of the specific methods introduced in the framework.

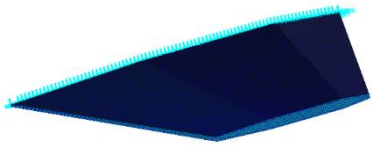

Fig. 5 Finite element model of the structure

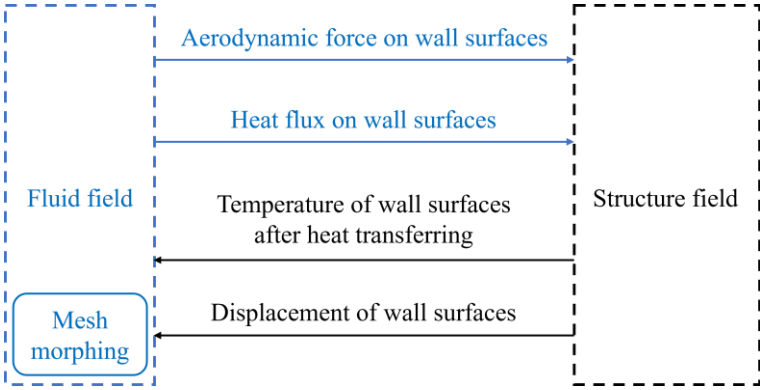

Fig. 6 Data transfer between subdisciplines

3.2.1 Mesh morphing technology based on RBF-TFI

For structured multi-block grids, which are suitable for viscous flow simulation of complex aerodynamic configurations, the radial basis functions (RBF) method has a high interpolation accuracy, but it is necessary to solve a group of linear equations about the weight coefficients, and the computational efficiency becomes extremely low when the grid size is large. Transfinite interpolation (TFI) method still has a high computational efficiency when the grid size is large, but the interpolation accuracy is low and the generalization is poor. Considering that the deformation of the internal grid points mainly depends on the boundary grid peaks of the block and the deformation accuracy of the grid block boundary is crucial, this paper adopts the RBF method to deform the boundary surfaces of the grid block. Subsequently, the deformation of the internal nodes of each mesh block is obtained by 3D-TFI technique. In summary, this paper adopts an RBF-TFI based mesh morphing technique to update the flow field mesh during analysis.

RBF is based on basis function superposition, which constructs an interpolation function based on some points in the space whose function values are known, and then interpolates the unknown points. The specific idea of the method is to use the function values of the known sample points to construct the function to calculate the function value at the point to be interpolated[25].

There are n known sample points in N-dimensional space with coordinates $(x_{i1}, x_{i2}, \cdots, x_{iN})$ and corresponding displacement function values W_i, where $i = 1, 2, \cdots, n$. It can be assumed that the approximation function at the coordinates $(x_1, x_2, \cdots, x_N)$ of any unknown point in this N-dimensional space is:

$$\overline{W} = \begin{bmatrix} 1 & x_1 & \cdots & x_N & \bar{b}_1 & \cdots & \bar{b}_n \end{bmatrix} \begin{bmatrix} c_1 \\ c_2 \\ \vdots \\ c_{N+1} \\ c_{N+2} \\ \vdots \\ c_{N+1+n} \end{bmatrix} = \bar{\mathbf{X}}\mathbf{c} \tag{6}$$

In which, $\bar{b}_i = \bar{r}_i^2 \ln(\bar{r}_i^2 + \varepsilon)$ is the form of the basis function chosen in this paper, and $c_1, c_2, \cdots c_{n+1+N}$ are the coefficient to be determined; ε is the given constant, which is generally different according to the characteristics of the surface where the interpolation point is located; $\varepsilon = 10^{-2} \sim 1$ for general flat surfaces and $\varepsilon = 10^{-6} \sim 10^{-5}$ for certain surfaces with singularities; x_{ip} is the p coordinate of the i sample point. The coefficients can be determined by the equations:

$$\begin{cases} \sum_{i=1}^{n} c_{N+1+i} = 0 \\ \sum_{i=1}^{n} c_{N+1+i} x_{ip} = 0 \quad p = 1, 2, \cdots, N \\ c_1 + \sum_{p=1}^{N} c_{p+1} x_{jp} + \sum_{i=1}^{n} c_{N+1+i} r_{ji}^2 \ln(r_{ji}^2 + \varepsilon) + h_j c_{N+1+j} = W_j \\ r_{ji}^2 = \sum_{p=1}^{N} (x_{jp} - x_{ip})^2 \quad j = 1, 2, \cdots, n;\ j \neq i \end{cases} \tag{7}$$

In equation (7), it is necessary to pre-given the weighting factor h_j for the j sample point. In this paper, all h_j is taken to be 0, so that the fitted function surface passes through the function value of all known sample points exactly.

The TFI[26] uses a Boolean sum of interpolating functions, and the displacement expression is as follows:

$$\boldsymbol{\Delta x}_{i,j,k} = U + V + W - UV - VW - UW + UVW \tag{8}$$

where $\boldsymbol{\Delta x}_{i,j,k} = [\Delta x_{i,j,k}, \Delta y_{i,j,k}, \Delta z_{i,j,k}]$, is the value of the displacement function at coordinate $\boldsymbol{x}_{i,j,k} = [x_{i,j,k}, y_{i,j,k}, z_{i,j,k}]$. The calculation equations of the univariate and composite variables can be easily found in relevant literatures.

3.2.2 Data interpolation techniques based on RBF

The Infinite Plate Spline (IPS) method is a commonly used displacement interpolation method based on RBF theory in fluid/structural coupling analysis. It should be noted that the known coordinates and known displacements in the IPS displacements come from the structural grids, while the unknown coordinates and the obtained displacements belong to the fluid mesh.

To ensure that loads are conserved before and after interpolation, the load interpolation equation can be derived from the displacement interpolation equation derived from the principle of conservation of energy (ENGY). This is the virtual work conservation method: the virtual work done on the respective grid displacements by the aerodynamic forces and the structural loads interpolated to the structure are equal.

The displacement of a fluid node $\mathbf{u}_K$ is related to the displacement of a structural grid $\mathbf{u}_G$:

$$\mathbf{u}_K = \mathbf{G}_{KG} \mathbf{u}_G \tag{9}$$

where $\boldsymbol{G}_{KG}$ is the displacement interpolation matrix of $\boldsymbol{u}_G$ to $\mathbf{u}_K$. Then, the virtual displacement can be written as:

$$\delta \mathbf{u}_K = \mathbf{G}_{KG} \delta \mathbf{u}_G \tag{10}$$

Thus, the virtual work of the aerodynamic and structural grids can be written as follows, respectively.

$$\delta W_K = \mathbf{F}_K^T \delta \mathbf{u}_K, \quad \delta W_G = \mathbf{F}_G^T \delta \mathbf{u}_G \tag{11}$$

The conservation of virtual work $\delta W_K = \delta W_G$ can be written as:

$$\mathbf{F}_K^T \delta \mathbf{u}_K = \mathbf{F}_G^T \delta \mathbf{u}_G \tag{12}$$

Substituting equation (10) into equation (12):

$$\mathbf{F}_G = \mathbf{G}_{KG}^T \mathbf{F}_K \tag{13}$$

where $\mathbf{G}_{KG}^T$ is the load interpolation matrix.

3.3 Methods comparison

The validation example is a horizontally placed rudder with a span of 265mm, a chord range of 740mm-350mm from its root to its tip, a sweep angle of 56°, a thickness of 60mm, and a profile shape of a single diamond. In order to verify the methodology used in the framework, a static aero-thermo-elastic analysis is carried out for the rudder, and the aerodynamic load and heat are compared with the results of engineering algorithms based on the third-order piston theory and the reference temperature method.

3.3.1 Example settings

The comparison model is shown in Fig. 7 and Fig. 8. The structural material properties and aerodynamic mesh boundary conditions are set as described in Section 3.1.1. The static heat accumulation analysis is carried out for 25 seconds under the longitudinal working condition of 15km altitude, 6Ma, and 6 degrees angle of attack (AoA).

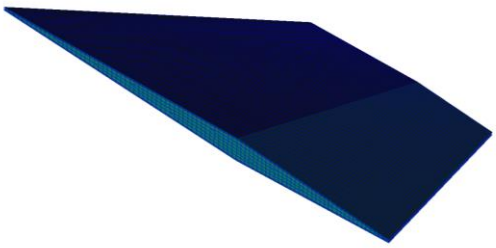

Fig. 7 Structural model for validation analysis

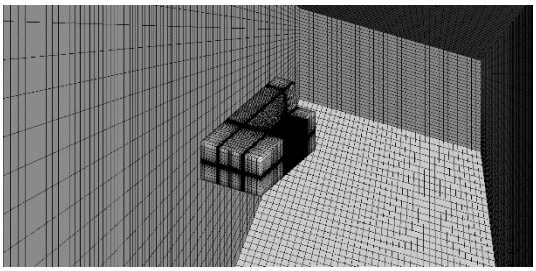

Fig. 8 Fluid mesh for validation analysis

3.3.2 Results comparison

As shown in Tab. 3, CFD shows higher pressure underneath, while there is not much difference on the upper surface in terms of aerodynamic load, for this example. The engineering algorithms are able to simulate the aerodynamic effects of the shock wave at the leading edge and the subsequent expansion wave of the two-dimensional flow in the airfoil profile, while the CFD method is able to capture the three-dimensional effect on top of that, and the distribution of aerodynamic load has a more pronounced spreading variation along the span direction.

In addition, the two methods are in general agreement in terms of aerodynamic-thermal results.

Tab. 3 Comparison of results

Time at 25s	From engineering algorithms	From CFD/CTD/CSD
Pressure (Pa)	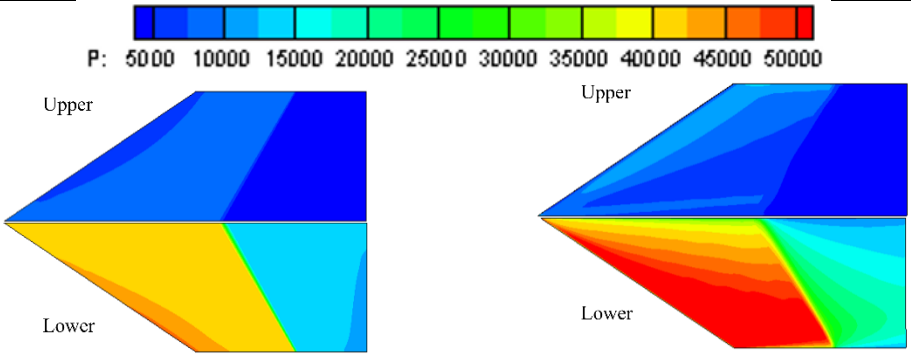	
Heat Flux (W/m^2)	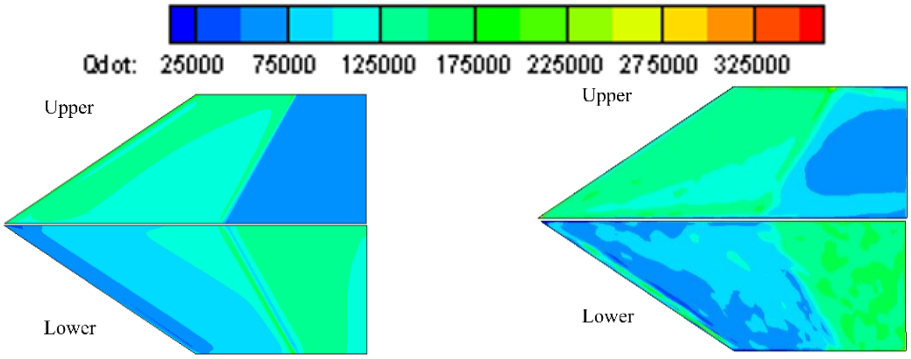	
Temperature (K)	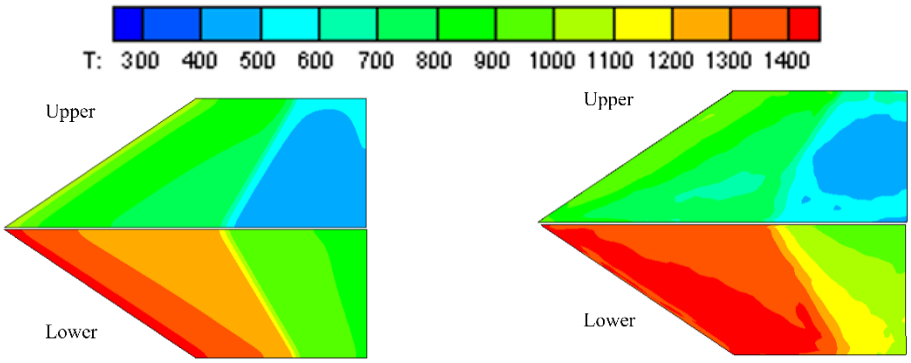	

As shown in Fig. 9 and Fig. 10, the CFD method captures the stagnation point on the lower surface due to the positive AoA, so that the region of the highest temperature of the near-wall airflow is not the leading edge but the region of the lower surface near the leading edge.

Besides, the fluid mesh in this paper is not in the form of a perfect half-mode on one side of the symmetry plane, allowing the CFD method to additionally capture the three-dimensional flow effect near the root profile and resulting in different aerodynamic load and heat flux distribution near the root on the upper surface compared with that from the engineering algorithms.

Since the results obtained from the CFD/CTD/CSD framework established in this paper are essentially the same as those derived from the engineering algorithms, the framework is used to analyze the full-vehicle scale example in the subsequent section.

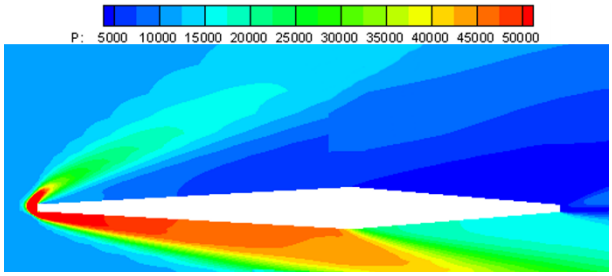

Fig. 9 Flow field pressure distribution near 1/2 span (side view)

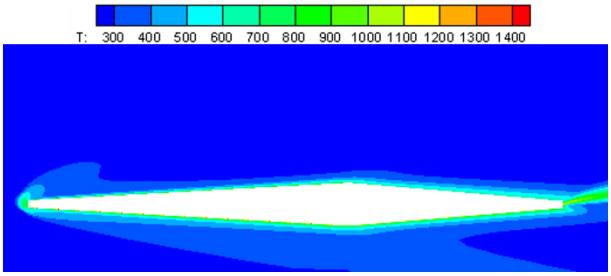

Fig. 10 Flow field Temperature distribution near 1/2 span (side view)

4 AERO-THERMO-ELASTIC ANALYSIS FOR ASSEMBLED RUDDERS

The full-assembly scale analysis model is described in Section 3.1. The maximum thickness of the rudders is 40 mm, the maximum chord length is 740 mm, the component span length is 266 mm, and the sweep angle is about 55 °. The 68s heat accumulation analysis is carried out under the static longitudinal condition of 15 km height, 6Ma and 6 ° AoA.

4.1 Calculated consumption

The total element number of fluid meshes for the half-mold assembly is about 2.44 million, and the structural finite element model of a single rudder has about 32,000 solid elements. The analysis program takes up about 28 cores and 40G of running memory to execute on a WIN 10 system. The related modules of structural analysis run fast, so the cost of program is mainly based on model pre-processing (such as calculating the mesh morphing matrix) and CFD operation. In the case of the existing pre-processing data, the time cost of one cycle is about 3 hours.

4.2 Results analysis

This section shows the simulation results for the key physical quantities of aero-thermo-elastic problems. All physical quantities in the following figures are shown in international standard units, unless there are annotations in figures.

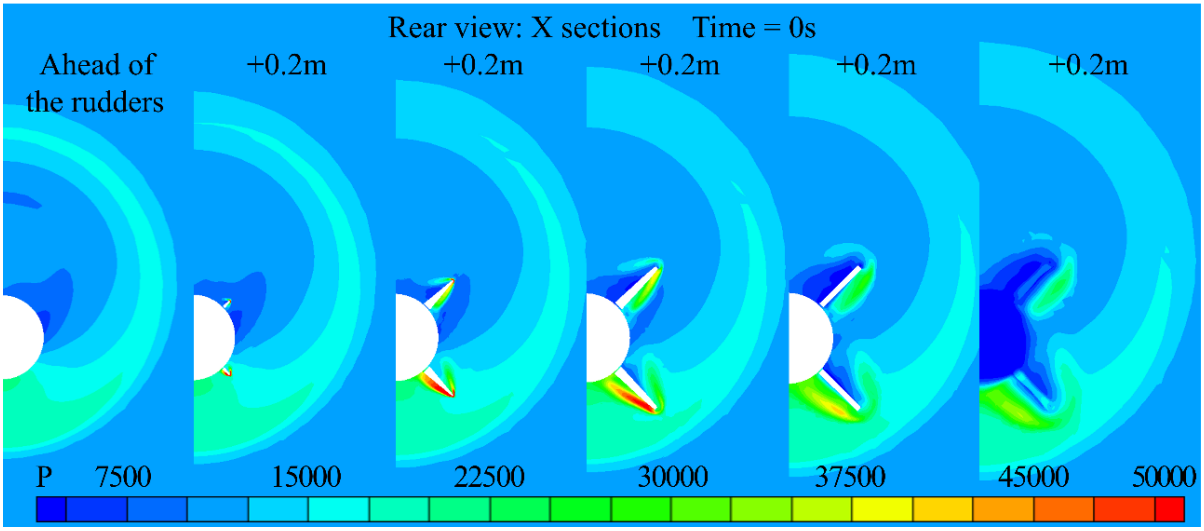

Fig. 11 The pressure of the flow field from the rear view

4.2.1 Characterization of the flow field

Fig. 11 shows the pressure distribution along the axial direction (x-direction) of the missile body on each flow field profile near the rudders, through the perspective of the rear view. And Fig. 12 illustrates the flow field characteristics on the near-wall y-direction profiles.

As shown in Fig. 11, due to the presence of a 6-degree AoA, the full-missile lift is mainly provided by the high pressure below the Rudder 2 and the body. Meanwhile, due to the relatively small lateral scale of the assembly, the flow has a significant three-dimensional effect, thus generating wingtip vortices for the two rudders, which are more pronounced in Rudder 2. Rudder 1, because of the 45-degree dihedral angle and the a positive AoA, the flow forms a low-pressure area on the upper surface near the missile body region from the leading edge, which gradually develops toward the wingtip with the direction of flow field movement.

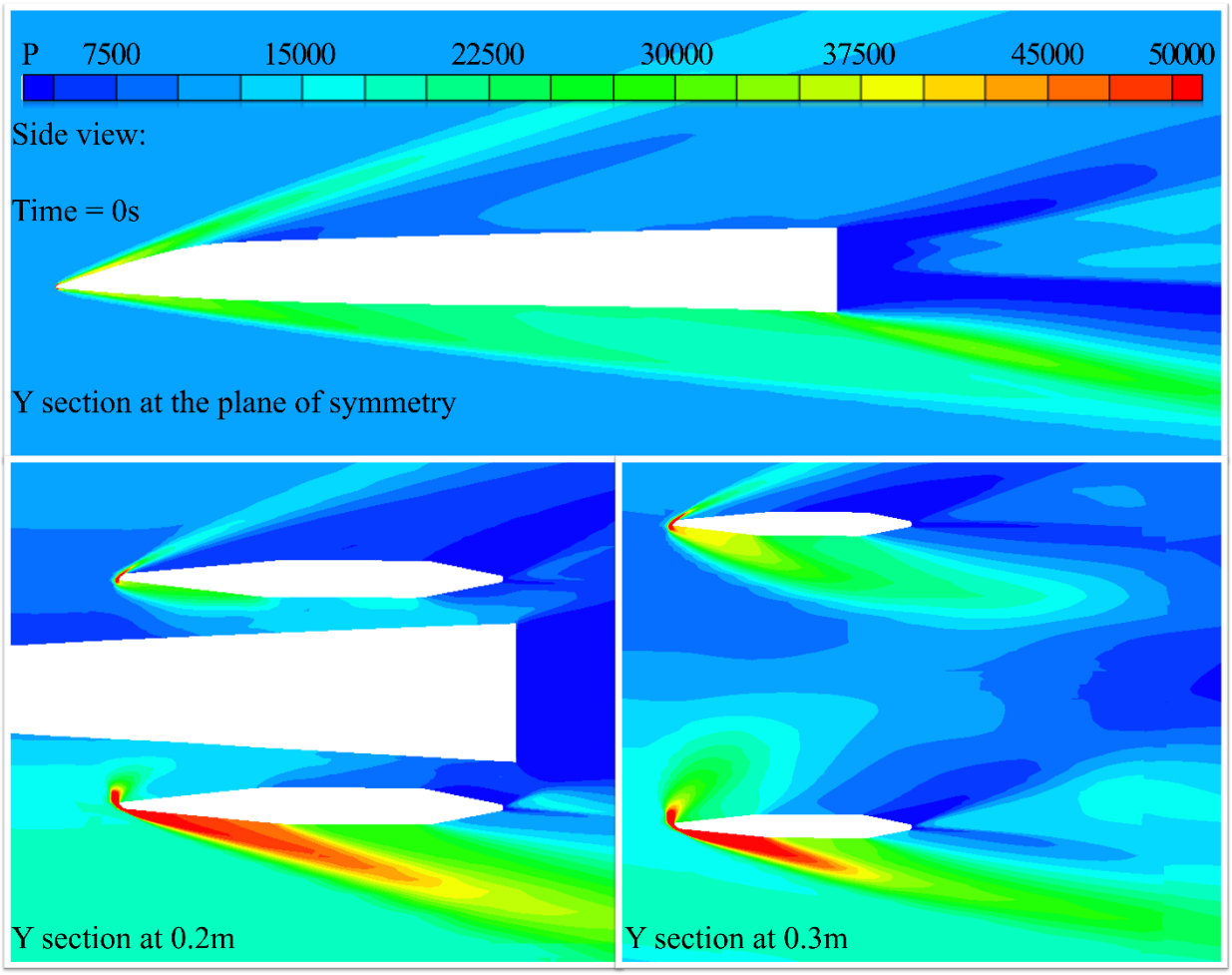

Fig. 12 The pressure of the flow field from the side view

4.2.2 Aero-thermo-elastic results

Fig. 13 shows the aerodynamic pressure considering heat transfer and structural deformation. It can be seen that the aerodynamic load distribution on Rudder 2 is larger than that on Rudder 1, which is caused by the combined effective angle of AoA and their dihedral angles. Rudder 2 is assembled near the high-pressure area as shown in Fig. 11, which can be clearly seen by CFD

method. The highest pressure is located on the lower surface of Rudder 2 near its leading edge, while there is a relevant smaller difference between the two rudders near their tailing edge.

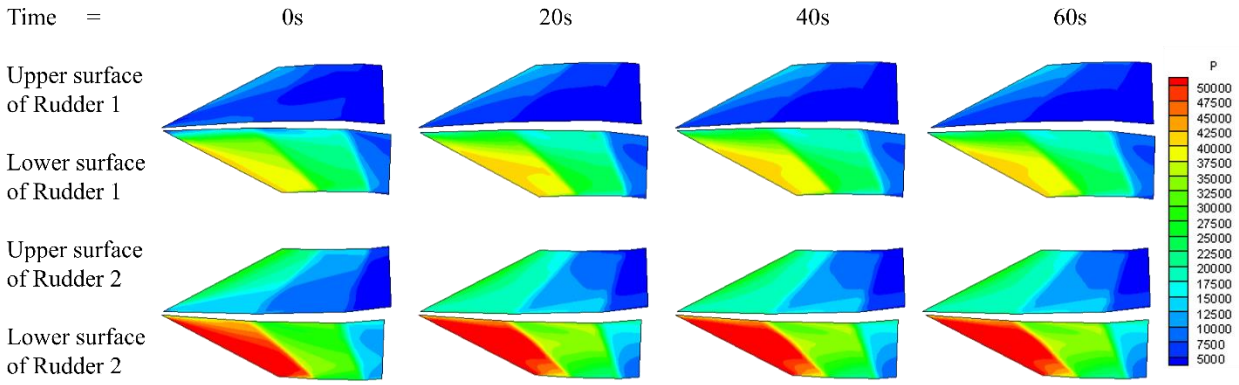

Fig. 13 Aerodynamic load distribution

Fig. 14 shows the aerodynamic temperature distribution on the upper and lower surfaces of the rudders. The highest temperature is located at the Rudder 1's tip profile near the leading edge because of the dihedral angle, while the lower surface of Rudder 2 bears the maximum temperature in the middle of its span.

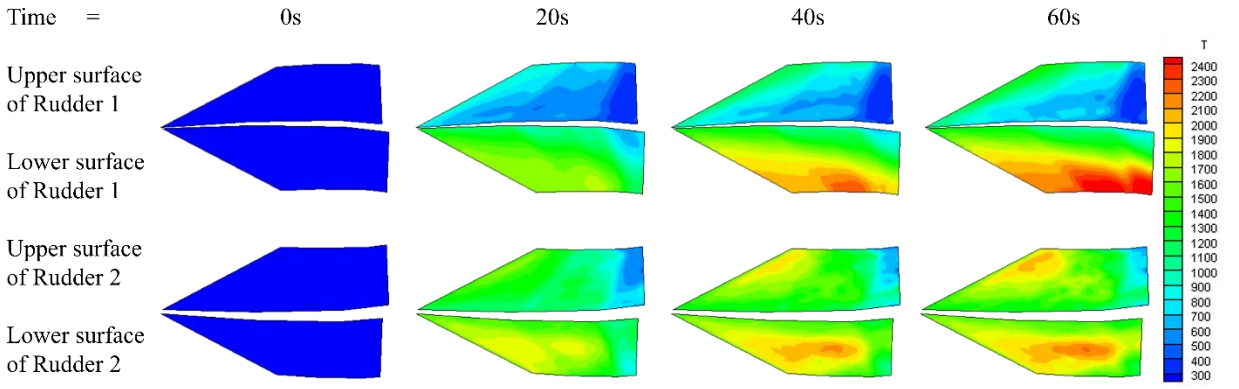

Fig. 14 Temperature distribution

As shown in Fig. 15, the aerodynamic heat flux at the leading edge is much larger than that at the tailing edge of the root profile for both of the rudders at first. However, with the aerodynamic heating, the surface temperature of the structure rises rapidly, and the temperature of the leading edge and the tip profile rises fastest which leads to the rapid decrease of heat flux in this area. At 60s, the heat flux distribution on the rudder surfaces is opposite to that at the beginning, especially for the lower surface of Rudder 1. Due to the constant low temperature set (300K) of the body wall in this paper, it has an effect on the heat flux on the root profiles of the rudders, making it higher than that at the middle of the rudders.

There is also an obvious heat flux difference between the two rudders, which means that the components of the same material are subjected to different thermal loads at the same time. It can be seen that an obvious area of heat dissipation occurs within 60s for Rudder 1. Due to the high

heat load, Rudder 1 needs a thicker thermal protection system (TPS) in order to ensure the structural stiffness throughout the whole task period. It may result in an increase in the weight of the structure, so it is more necessary to optimize the structure of Rudder 1, taking thermal effects into account. It is also noteworthy that the surfaces obtain extremely strong heat flux which may cause ablation of the TPS.

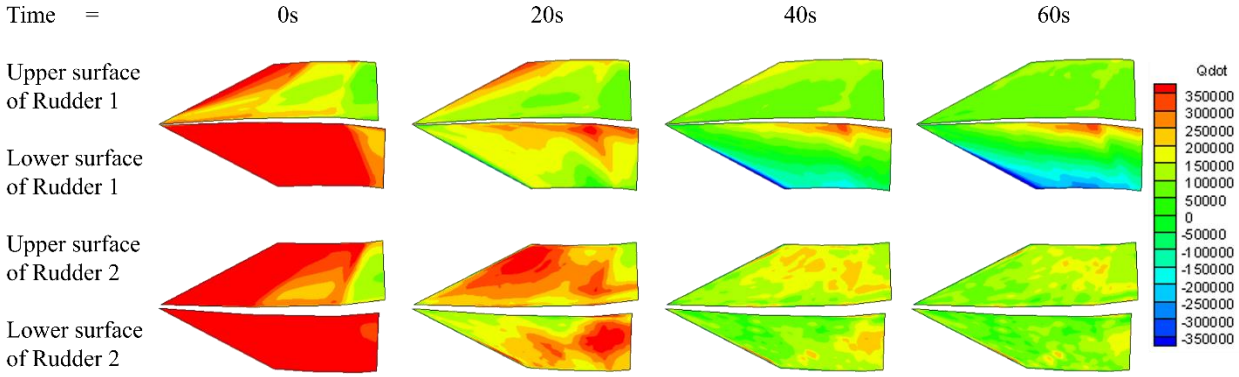

Fig. 15 Heat flux distribution

Fig. 16 shows the thermal displacement of the monitoring points on tip profiles, which is important to the total deformation response of the structure. In Fig. 16, it can be seen that the thermal deformation of Rudder 1 increases continuously while that of Rudder 2 shows slight decrease. The monitoring points' thermal deformation at the tip of Rudder 1 increases continuously while that of Rudder 2 tends to converge, which indicates that although the surface heat flux on Rudder 1 shows negative value around 60s, its internal temperature is still rising, while that of Rudder 2 tends to be stable with large area of low heat flux input. These phenomena imply that different assembly positions under specific working conditions will affect the load bearing of the structure. Therefore, it is necessary to analyze and design the same components at different locations separately according to the specific flight trajectory.

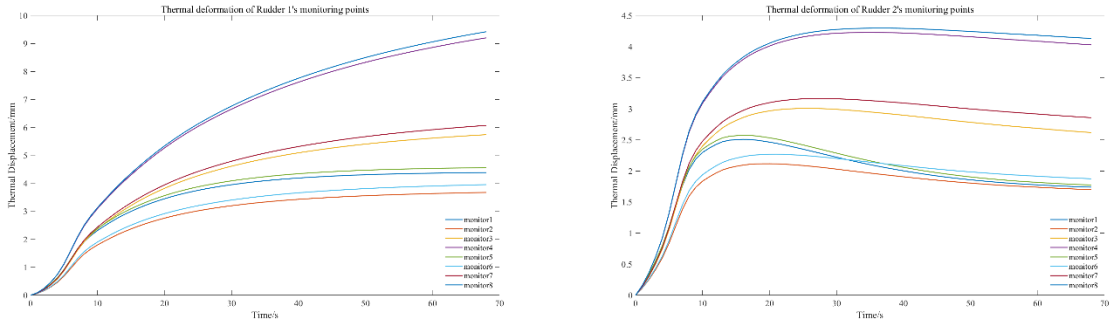

Fig. 16 Thermal deformation of the structural monitor points

5 CONCLUSIONS

This paper establishes a FTSI framework applicable to full-vehicle scale analysis based on the CFD/CTD/CSD method, demonstrates the aero-thermo-elastic effects of special-assembled shape

factors that cannot be shown by the engineering algorithms, and discusses the influence of these factors on the design of hypersonic vehicles through the simulation results.

The results show that the full-vehicle CFD calculations provide more accurate aerodynamic and aerothermal data, which are significantly different from the engineering algorithms in terms of the magnitude and distribution of aerodynamic load. It will make the elastic displacement obtained by the engineering algorithm too conservative. In the full-vehicle analysis, the load and temperature distribution of components, such as rudders, are much more complex than those shown by the engineering algorithms due to the influence of the surface temperature distribution of the body and the negative pressure region of its wake flow. This means that the actual situation of the local flow near the components is significantly different from the simplified assumptions, so it is difficult to obtain accurate aerodynamic heating distribution by using the engineering algorithm. Therefore, the high-precision multi-field coupling analysis method based on CFD/CTD/CSD is of great significance for the design of hypersonic vehicles. However, its computational efficiency is far less than that of engineering algorithms, making it difficult to be directly extended to the practice of optimization design.

In the next stage, the development of data-driven computational methods that synthesize high-precision CFD data and high-efficiency engineering algorithms is needed. Quantifying the impact of design parameters on aero-thermo-elastic response in each sub-discipline, and applying them to the optimized design of component structures is a promising research direction.

REFERENCES

[1] Sziroczak D., Smith H. A review of design issues specific to hypersonic flight vehicles. *Progress in Aerospace Sciences* 2016;**84**:1–28. Doi: 10.1016/j.paerosci.2016.04.001.

[2] Culler Adam J., McNamara Jack J. Impact of Fluid-Thermal-Structural Coupling on Response Prediction of Hypersonic Skin Panels. *AIAA Journal* 2011;**49**(11):2393–406. Doi: 10.2514/1.J050617.

[3] Subrahmanyam Prabhakar. Development of an Interactive Hypersonic Flow Solver Framework for Aerothermodynamic Analysis. *Engineering Applications of Computational Fluid Mechanics* 2008;**2**(4):436–55. Doi: 10.1080/19942060.2008.11015243.

[4] Daub Dennis, Willems Sebastian, Gülhan Ali. Experiments on aerothermoelastic fluid–structure interaction in hypersonic flow. *Journal of Sound and Vibration* 2022;**531**:116714. Doi: 10.1016/j.jsv.2021.116714.

[5] Mack Andreas. Aerothermodynamic behaviour of a generic nosecap model including thermomechanical structural effects. *Aerospace Science and Technology* 2007;**11**(5):386–95. Doi: 10.1016/j.ast.2007.01.002.

[6] Influence of surface nanostructures on the catalytic recombination of hyperthermal non-equilibrium flow. *Physics of Fluids* 2023;**35**(4):042108. Doi: 10.1063/5.0145963.

[7] Li Jia-Wei, Wang Jiang-Feng. An improved hybrid lattice Boltzmann flux solver for 3D integrated hypersonic fluid-thermal-structural analysis. *Int J Mod Phys B* 2020;**34**(14n16):2040072. Doi: 10.1142/S021797922040072X.

[8] Song Zhi-Guang, Li Feng-Ming. Aerothermoelastic analysis of nonlinear composite laminated panel with aerodynamic heating in hypersonic flow. *Composites Part B: Engineering* 2014;**56**:830–9. Doi: 10.1016/j.compositesb.2013.09.019.

[9] Comas Edgardo, Legnani Walter. A preliminary study on the non-linear behavior of hypersonic flow. *Chaos, Solitons & Fractals* 2017;**105**:51–9. Doi: 10.1016/j.chaos.2017.10.010.

[10] Wang Wenrui, Wang Zhengfa, Wang Shuai, Deng Huan, Li Hanlin. Ablation Behavior of Rudder Wing Structure in Hypersonic Environment. *J Aerosp Eng* 2023;**36**(4):04023026. Doi: 10.1061/JAEEEZ.ASENG-4681.

[11] Huang Daning, Rokita Tomer, Friedmann Peretz P. Integrated Aerothermoelastic Analysis Framework with Application to Skin Panels. *AIAA Journal* 2018;**56**(11):4562–81. Doi: 10.2514/1.J056677.

[12] Munk David J., Verstraete Dries, Vio Gareth A. Effect of fluid-thermal–structural interactions on the topology optimization of a hypersonic transport aircraft wing. *Journal of Fluids and Structures* 2017;**75**:45–76. Doi: 10.1016/j.jfluidstructs.2017.08.007.

[13] Jiang Guoqing, Li Fengming. Aerothermoelastic analysis of composite laminated trapezoidal panels in supersonic airflow. *Composite Structures* 2018;**200**:313–27. Doi: 10.1016/j.compstruct.2018.05.138.

[14] Liu Wenjian, Deng Lianbing, Cai Zhiming, Li Daming, Rahimi Alireza. Impact of in-plane follower force on the frequency response of the hybrid angle-ply laminated system via dynamic simulation and generalized differential quadrature framework. *Engineering with Computers* 2022;**38**(S5):3743–60. Doi: 10.1007/s00366-020-01215-4.

[15] Shu C., Yeo K.S., Yao Q. On the performance of three iterative methods for solution of GDQ algebraic equations. *Computer Methods in Applied Mechanics and Engineering* 1998;**167**(1–2):1–15. Doi: 10.1016/S0045-7825(98)00103-0.

[16] Zhang Wulin, Liu Zirui, Liang Zeyu, Oslub Khaled, Safarpour Hamed. A comprehensive computer simulation of the size-dependent sector or complete microsystem via two-dimensional generalized differential quadrature method. *Engineering with Computers* 2022;**38**(S5):4239–55. Doi: 10.1007/s00366-021-01440-5.

[17] Qin Mengzhu, Cheng Meng, Mian Haris Hameed, Wang Gang. Fluid-thermal-structural interaction simulation with coupled CFD/CSD method. *2016 13th International Bhurban Conference on Applied Sciences and Technology (IBCAST)*; Islamabad, Pakistan; 2016. p. 440–6.

[18] Bisplinghoff R. L. Some Structural and Aeroelastic Considerations of High-Speed Flight The Nineteenth Wright Brothers Lecture. *Journal of the Aeronautical Sciences* 1956;**23**(4):289–321. Doi: 10.2514/8.3557.

[19] Xie Fangtao, Qu Yegao, Guo Qiwei, Zhang Wenming, Peng Zhike. Nonlinear flutter of composite laminated panels with local non-smooth friction boundaries. *Composite Structures* 2019;**223**:110934. Doi: 10.1016/j.compstruct.2019.110934.

[20] Lin Huagang, Cao Dengqing, Shao Chonghui, Xu Yuqian. Studies for aeroelastic characteristics and nonlinear response of FG-CNT reinforced composite panel considering the transient heat conduction. *Composite Structures* 2018;**188**:470–82. Doi: 10.1016/j.compstruct.2018.01.028.

[21] Chai Yuyang, Song Zhiguang, Li Fengming. Investigations on the aerothermoelastic properties of composite laminated cylindrical shells with elastic boundaries in supersonic airflow based on the Rayleigh–Ritz method. *Aerospace Science and Technology* 2018;**82–83**:534–44. Doi: 10.1016/j.ast.2018.09.040.

[22] Zhang L.W., Song Z.G., Liew K.M. Modeling aerothermoelastic properties and active flutter control of nanocomposite cylindrical shells in supersonic airflow under thermal environments. *Computer Methods in Applied Mechanics and Engineering* 2017;**325**:416–33. Doi: 10.1016/j.cma.2017.07.014.

[23] Quan Enqian, Xu Min, Yao Weigang, Cheng Xiang. Analysis of the post-flutter aerothermoelastic characteristics of hypersonic skin panels using a CFD-based approach. *Aerospace Science and Technology* 2021;**118**:107076. Doi: 10.1016/j.ast.2021.107076.

[24] Huo Lin, Cheng Xing-Hua, Yang Tao. Aerothermoelastic response analysis for C/SiC panel of ceramic matrix composite shingle thermal protection system. *Advances in Space Research* 2015;**55**(9):2352–71. Doi: 10.1016/j.asr.2015.02.008.

[25] Harder Robert L., Desmarais Robert N. Interpolation using surface splines. *Journal of Aircraft* 1972;**9**(2):189–91. Doi: 10.2514/3.44330.

[26] Dyken Christopher, Floater Michael S. Transfinite mean value interpolation. *Computer Aided Geometric Design* 2009;**26**(1):117–34. Doi: 10.1016/j.cagd.2007.12.003.

COPYRIGHT STATEMENT

The authors confirm that they, and/or their company or organisation, hold copyright on all of the original material included in this paper. The authors also confirm that they have obtained permission from the copyright holder of any third-party material included in this paper to publish it as part of their paper. The authors confirm that they give permission, or have obtained permission from the copyright holder of this paper, for the publication and public distribution of this paper as part of the IFASD 2024 proceedings or as individual off-prints from the proceedings.